

# A statistical model of three-dimensional anisotropy and intermittency in strong Alfvénic turbulence

A. Mallet<sup>1,2★</sup> and A. A. Schekochihin<sup>2,3</sup>

<sup>1</sup>Space Science Center, University of New Hampshire, Durham, NH 03824, USA

<sup>2</sup>Rudolf Peierls Centre for Theoretical Physics, University of Oxford, Oxford OX1 3NP, UK

<sup>3</sup>Merton College, Oxford OX1 4JD, UK

Accepted 2016 December 10. Received 2016 November 28; in original form 2016 May 24

## ABSTRACT

We propose a simple statistical model of three-dimensionally anisotropic, intermittent, strong Alfvénic turbulence, incorporating both critical balance and dynamic alignment. Our model is based on log-Poisson statistics for Elsasser-field increments *along* the magnetic field. We predict the scalings of Elsasser-field conditional two-point structure functions with point separations in all three directions in a coordinate system locally aligned with the direction of the magnetic field and of the fluctuating fields and obtain good agreement with numerical simulations. We also derive a scaling of the parallel coherence scale of the fluctuations,  $l_{\parallel} \propto \lambda^{1/2}$ , where  $\lambda$  is the perpendicular scale. This is indeed observed for the bulk of the fluctuations in numerical simulations.

**Key words:** MHD – turbulence – solar wind.

## 1 INTRODUCTION

Turbulent plasma fills most of the visible Universe, and can be measured directly by spacecraft in the solar wind (Bruno & Carbone 2013). In many situations, a strong mean magnetic field  $\mathbf{B}_0$  is present, which ensures that on scales longer than the ion gyroradius, Alfvénically polarized fluctuations decouple from the compressive fluctuations and satisfy the equations of reduced magnetohydrodynamics (RMHD; Schekochihin et al. 2009). These can be written in terms of Elsasser variables  $\mathbf{z}_{\pm} = \mathbf{u}_{\pm} \pm \mathbf{b}_{\pm}$ , where  $\mathbf{u}_{\pm}$  and  $\mathbf{b}_{\pm}$  are the velocity and magnetic-field (in velocity units) perturbations perpendicular to the background magnetic field  $\mathbf{B}_0$ :

$$\partial_t \mathbf{z}_{\pm} \mp v_A \partial_z \mathbf{z}_{\pm} + \mathbf{z}_{\pm} \cdot \nabla_{\perp} \mathbf{z}_{\pm} = -\nabla_{\perp} p, \quad (1)$$

where the pressure  $p$  can be determined from  $\nabla_{\perp} \cdot \mathbf{z}_{\pm} = 0$ , the Alfvén speed is  $v_A = |\mathbf{B}_0|$  and  $\mathbf{B}_0$  is in the  $z$  direction.

The turbulent state described by equations (1) is anisotropic with respect to the direction of the local magnetic field, in full MHD simulations with a strong guide field (e.g. Oughton, Priest & Matthaeus 1994; Matthaeus et al. 1996, 1998; Cho & Vishniac 2000; Maron & Goldreich 2001; Bigot, Galtier & Politano 2008), direct numerical simulations of RMHD (e.g. Shebalin, Matthaeus & Montgomery 1983; Oughton, Dmitruk & Matthaeus 2004; Chen et al. 2011; Beresnyak 2015; Mallet et al. 2016) and also in the solar wind (e.g. Horbury, Forman & Oughton 2008; Podesta 2009; Wicks et al. 2010; Chen et al. 2011). This anisotropic state can be understood on the basis of the critical-balance conjecture

(Goldreich & Sridhar 1995, 1997): the nonlinear  $\tau_{nl}^{\pm}$  and linear  $\tau_A^{\pm} \doteq l_{\parallel}^{\pm}/v_A$  times should be similar at every scale in the inertial range, where  $l_{\parallel}^{\pm}$  is the coherence length of the fluctuations along the magnetic-field lines. This allows one to equate the cascade time to either of these times, and therefore, by an argument following Kolmogorov (1941), the constancy of the energy flux through parallel scales

$$\epsilon^{\pm} \sim \frac{(\delta z_{\perp}^{\pm})^2}{\tau_c} \sim \frac{(\delta z_{\perp}^{\pm})^2 v_A}{l_{\parallel}^{\pm}} \sim \text{const}, \quad (2)$$

implying that  $(\delta z_{\perp}^{\pm})^2 \sim l_{\parallel}^{\pm}(\epsilon^{\pm}/v_A)$ , and hence a ‘parallel spectral index’ of  $-2$ , regardless of the details of the nonlinear interactions. This is, indeed, observed in the simulations and in the measurements of the solar wind cited above.

As is evident in the form of the nonlinear term in equations (1), only  $\mathbf{z}_{\pm}$  with a gradient in the direction of  $\mathbf{z}_{\pm}$  gives rise to a non-zero contribution to the RMHD nonlinearity. Combined with the 2D-solenoidal nature of the Elsasser fields,  $\nabla_{\perp} \cdot \mathbf{z}_{\pm} = 0$ , this means that *dynamic alignment* (Beresnyak & Lazarian 2006; Boldyrev 2006) of their fluctuation vectors to within a small angle  $\theta$  of each other will decrease the nonlinearity by a factor of  $\sin \theta$ . The definition of the nonlinear time must take this into account:

$$\tau_{nl}^{\pm} \doteq \frac{\lambda}{\delta z_{\perp}^{\pm} \sin \theta}, \quad (3)$$

where  $\lambda$  is the perpendicular coherence length. If  $\theta$  depends on  $\delta z_{\perp}^{\pm}$  and  $\lambda$  in a non-trivial manner, this will affect the scaling behaviour of the nonlinear time and, therefore, the scaling of the fluctuation amplitudes conditional on perpendicular scale  $\lambda$ ,  $\delta z_{\perp}^{\pm}$ . Here and

★ E-mail: [alfred.mallet@unh.edu](mailto:alfred.mallet@unh.edu)

everywhere, we will assume that the turbulence is ‘balanced’, i.e.  $\epsilon^+ \sim \epsilon^-$  and so  $\delta z_\perp^+ \sim \delta z_\perp^-$ ,  $l_\parallel^+ \sim l_\parallel^-$ , etc.

The alignment of the fields can be linked to anisotropy of sheet-like turbulent structures within the plane perpendicular to the mean magnetic field (Boldyrev 2006). The distance field lines wander in this perpendicular plane as a result of a  $\delta z_\perp^\pm$  fluctuation is

$$\xi \sim l_\parallel \frac{\delta z_\perp^\pm}{v_A}. \quad (4)$$

Since  $l_\parallel$ , by definition, is the coherence length along the field line, the fluctuations must be coherent in their own direction (the ‘fluctuation direction’) up to a distance of at least  $\xi$ . However, since the fluctuation is comprised of a mixture of both Elsasser fields  $\delta z_\perp^+$  and  $\delta z_\perp^-$ , the fluctuation direction is only defined up to the angle  $\theta$  between them, and we can therefore estimate the aspect ratio of the correlated structures within the perpendicular plane as

$$\frac{\lambda}{\xi} \sim \sin \theta. \quad (5)$$

Combining equations (4) and (5) with equation (3) gives us back the critical balance conjecture:

$$\frac{\delta z_\perp l_\parallel}{\xi v_A} \sim \frac{\tau_A}{\tau_{nl}} \sim 1. \quad (6)$$

In combination with the parallel anisotropy, the above argument implies that the turbulence may be 3D anisotropic with respect to an instantaneous local basis defined by the directions of the mean magnetic field, the fluctuations and the direction perpendicular to both. This was indeed confirmed in numerical simulations (Verdini & Grappin 2015; Mallet et al. 2016) and in the solar wind (Chen et al. 2012). Thus, the 3D anisotropy of RMHD turbulence can be understood as arising from a combination of critical balance (Goldreich & Sridhar 1995) and dynamic alignment (Boldyrev 2006).

Another distinctive feature of RMHD turbulence (in which it resembles hydrodynamic turbulence; see e.g. Frisch 1995) is intermittency, i.e. the fact that the distribution of turbulent random fields is not scale-invariant (see Chandran, Schekochihin & Mallet 2015 and references therein). It has become clear in recent years that intermittency is deeply intertwined with the physics of critical balance and dynamic alignment. For example, Mallet, Schekochihin & Chandran (2015) showed that, while nearly every random variable in numerically simulated RMHD turbulence is highly intermittent, the critical balance parameter  $\chi \doteq \tau_A/\tau_{nl}$  has a distribution that is scale-invariant in the inertial range – as long as dynamic alignment is included in the definition of  $\tau_{nl}$  as in equation (3). Moreover, it was shown in the same paper that the dynamic alignment angle was anticorrelated with amplitude at each given scale, i.e. the joint distribution of the turbulent random variables is highly non-trivial. Mallet et al. (2016) then measured the intermittency of the turbulence in the local basis defined by the directions of the mean magnetic field, the fluctuations and the direction perpendicular to both, and found the intermittency (quantified by structure-function scaling exponents) to be different in every direction.

In view of this emerging evidence, it is essential to develop holistic theories that combine realistic treatments of critical balance and dynamic alignment with models for the intermittency of the turbulent fluctuations. Recently, a new theory of intermittent RMHD turbulence was proposed (Chandran et al. 2015), which accurately predicted the scalings measured in the perpendicular direction by Mallet et al. (2016), by incorporating intermittency, critical balance and dynamic alignment into a physical model of the collisions of Alfvénic structures. In this paper, we will take another approach and

use these phenomena to propose a statistical model of the ‘RMHD turbulent ensemble’, further constrained by assumptions about the geometrical structure of the turbulent fluctuations, and leading to prediction of the scalings in the perpendicular, parallel and fluctuation directions. We will begin by proposing a joint distribution of the relevant turbulent variables, and then fix all the parameters of this model by using physically motivated conjectures.

## 2 RMHD ENSEMBLE

Suppose that we can meaningfully model the turbulent system as an ensemble of ‘structures’ or ‘fluctuations’, each defined by joint realizations of the following random variables:

$$\begin{aligned} \delta z &: \text{field amplitude,} \\ \lambda &: \text{perpendicular scale,} \\ l_\parallel &: \text{parallel scale,} \\ \xi &: \text{fluctuation – direction scale.} \end{aligned} \quad (7)$$

We have made the significant simplification that we do not need two separate amplitudes  $\delta z_\perp^\pm$ ; i.e. we have restricted ourselves to the case of overall balanced turbulence, and assume that even locally,  $\delta z_\perp^+ \sim \delta z_\perp^- \sim \delta z$ .

### 2.1 Joint probability distribution

Picking one particular structure from this ‘RMHD turbulent ensemble’ corresponds to sampling the joint distribution  $P(\delta z, \lambda, l_\parallel, \xi)$ . Conditional structure functions, which can be measured in a real (or numerically simulated) turbulent system (Mallet et al. 2016), correspond to moments of the conditional probability distributions  $P(\delta z|\lambda)$ ,  $P(\delta z|l_\parallel)$ ,  $P(\delta z|\xi)$ . We will therefore propose a particular functional form for the joint distribution  $P(\delta z, \lambda, l_\parallel, \xi)$  of our model ensemble and then use this to calculate the conditional distributions in order to predict the scalings of the conditional structure functions. It will turn out that, with some additional assumptions, we can treat  $\xi$  as a dependent variable, so we remove it from our consideration for now.

We will also need some global properties of the system, which we will treat as non-random:

$$\begin{aligned} \epsilon &: \text{global cascade rate,} \\ v_A &: \text{Alfvén speed,} \\ L_\perp &: \text{perpendicular outer scale,} \\ L_\parallel &: \text{parallel outer scale,} \\ \overline{\delta z} &: \text{outer – scale fluctuation amplitude.} \end{aligned} \quad (8)$$

We stress that the assumption that these quantities are non-random – especially in the case of  $\overline{\delta z}$  – is a significant idealization, but we believe this to be acceptable because none of them is scale dependent.<sup>1</sup> To simplify further calculations, we define normalized random variables

$$\delta \hat{z} = \frac{\delta z}{\overline{\delta z}}, \quad \hat{\lambda} = \frac{\lambda}{L_\perp}, \quad \hat{l}_\parallel = \frac{l_\parallel}{L_\parallel}, \quad \hat{\xi} = \frac{\xi}{L_\perp}. \quad (9)$$

<sup>1</sup> In general,  $\overline{\delta z}$  may be a scale-independent random variable, whose distribution is possibly non-universal and dependent on the details of the outer-scale energy injection. However, in Section 5.2, we shall see that treating it as non-random is at least not an outrageous idealization:  $\overline{\delta z}$  can be fit by a single constant, a few times the rms value of the Elsasser field.

**Conjecture 1.** *The fluctuation amplitudes can be modelled as*

$$\delta \hat{z} = \beta^q, \quad (10)$$

where  $q$  is a non-negative random integer,  $\beta$  is a constant,  $0 \leq \beta \leq 1$  and the joint probability distribution of  $q$ ,  $\hat{l}_\parallel$  and  $\hat{\lambda}$  has density

$$P(q, \hat{l}_\parallel, \hat{\lambda}) = \frac{\mu^q}{q!} e^{-\mu} f\left(\frac{\hat{l}_\parallel}{\hat{\lambda}^\alpha}\right), \quad (11)$$

where  $\mu = \mu(\hat{l}_\parallel)$ ,  $\alpha$  is a constant parameter and  $f$  is some function.

The unknown function  $f$  (which, it will turn out, we do not need to know, as long as it satisfies certain constraints) parametrizes the anisotropy. We will examine the quality of this parametrization in Section 6. The rest of the functional form of  $P$  can be motivated by the following argument.

## 2.2 Log-Poisson statistics

Let us calculate the conditional distribution  $P(q|\hat{l}_\parallel)$  from the model (11) (this is a distribution of Elsasser-field increments across a fixed parallel point separation  $l_\parallel$ ). Since  $\mu$  is not a function of  $\hat{\lambda}$ , we may integrate equation (11) over  $\hat{\lambda}$  and obtain

$$P(q|\hat{l}_\parallel) = \frac{P(q, \hat{l}_\parallel)}{P(\hat{l}_\parallel)} = \frac{\int_0^1 f(\hat{l}_\parallel/\hat{\lambda}^\alpha) d\hat{\lambda}}{P(\hat{l}_\parallel)} \frac{\mu^q}{q!} e^{-\mu}. \quad (12)$$

Summing equation (11) over  $q$ , we obtain

$$P(\hat{l}_\parallel, \hat{\lambda}) = f\left(\frac{\hat{l}_\parallel}{\hat{\lambda}^\alpha}\right), \quad (13)$$

whence, integrating over  $\hat{\lambda}$ , we find

$$P(\hat{l}_\parallel) = \int_0^1 f\left(\frac{\hat{l}_\parallel}{\hat{\lambda}^\alpha}\right) d\hat{\lambda}. \quad (14)$$

Therefore, from equation (12),

$$P(q|\hat{l}_\parallel) = \frac{\mu^q}{q!} e^{-\mu}, \quad (15)$$

which is a Poisson distribution with mean  $\mu$ .

Historically, the Poisson distribution as a model for the distribution of the logarithm of the fluctuation amplitude was used very successfully in hydrodynamic turbulence (Dubrulle 1994; She & Leveque 1994; She & Waymire 1995). Moreover, there is recent direct observational evidence of the solar-wind turbulence being at least consistent with log-Poisson statistics (Zhdankin, Boldyrev & Chen 2016b). The intermittency model of Chandran et al. (2015), which correctly predicts the perpendicular scalings of numerical RMHD turbulence, also used a log-Poisson model. An attractive physical interpretation of the log-Poisson model is that, as each fluctuation cascades to smaller  $\lambda$  and  $l_\parallel$ , it undergoes an integer number  $q$  of ‘modulation defects’, each of which is modelled as reducing the amplitude by a factor  $\beta$  (see equation 10). In Chandran et al. (2015), these defects were interpreted as collisions between unaligned Alfvénic wave packets.<sup>2</sup> Whereas

Chandran et al. (2015) posited a log-Poisson distribution for fluctuation amplitudes  $\delta z_\lambda$  conditioned on the perpendicular scale  $\lambda$  (i.e. Elsasser-field increments across perpendicular point separations  $\lambda$ ), we have here conjectured a log-Poisson distribution for  $\delta z_{l_\parallel}$  conditioned on the parallel scale  $l_\parallel$  (field increments across parallel separations  $l_\parallel$ ). This can be justified in the following way.

For the purposes of understanding intermittency, the constant-flux assumption (2) can turn into a critically balanced RMHD version of the refined-similarity hypothesis (Kolmogorov 1962):

$$\frac{\delta z_{l_\parallel}^2 v_A}{l_\parallel} \sim \epsilon_{l_\parallel}, \quad (16)$$

where  $\epsilon_{l_\parallel}$  is the dissipation rate averaged over scale  $l_\parallel$ , but fluctuating over the entire box of length  $L_\parallel$ . The global mean of this dissipation rate the Kolmogorov energy flux  $\langle \epsilon_{l_\parallel} \rangle = \epsilon_{L_\parallel} = \epsilon$ , independent of scale. One might then argue, following Kolmogorov (1962), that, refining the outer scale  $L_\parallel$  by a factor  $a < 1$ , we must have

$$\epsilon_{aL_\parallel} = \epsilon_{L_\parallel} W_1 = \epsilon W_1, \quad (17)$$

where  $W_1$  is a positive random variable with  $\langle W_1 \rangle = 1$ . Iterating this procedure, we may find that at any smaller scale  $l_\parallel = a^k L_\parallel$ ,

$$\epsilon_{l_\parallel} = \epsilon \prod_{i=1}^k W_i, \quad (18)$$

where  $W_i$ ’s are all independent and identically distributed, with  $\langle W_i \rangle = 1$ . Since the distribution of  $\epsilon_{l_\parallel}$  cannot depend on the (arbitrary) refinement constant  $a$ , we must be able to represent  $\epsilon_{l_\parallel}$  as a product of an arbitrary number of these  $W_i$ ’s and so the distribution of  $\log \epsilon_{l_\parallel}$  must be infinitely divisible. Finally, since, by equation (16),  $\epsilon_{l_\parallel} \propto \delta z_{l_\parallel}^2$ ,  $\log \delta z_{l_\parallel}$  must also be infinitely divisible.<sup>3</sup> The logarithms of the amplitudes are therefore described by a Lévy process, which can always be written as the sum of a Gaussian process, a superposition of compound Poisson processes, and a non-random component (Sato 2013). The Gaussian part is ruled out because it leads to a mathematically impossible scaling of structure functions (Frisch 1995), and the simplest possible compound Poisson distribution is just a Poisson distribution.

Thus, the log-Poisson model is at least reasonable physically, mathematically and observationally (in Section 5.2, we will examine how well it fits numerical data). We now have an explicit joint distribution of the turbulent random variables, equation (11), which involves unknown parameters  $\alpha$  and  $\beta$  and unknown functions  $\mu$  and  $f$ . In order to calculate the scalings of the conditional structure functions, these need to be determined or constrained using further physically motivated conjectures.

## 3 FINDING $\mu$ AND $\alpha$ : A TURBULENCE OF FLUX SHEETS

Taking some inspiration from She & Leveque (1994), we consider the most intense structures in our turbulent ensemble (i.e. those with  $q = 0$ ) and assume that they are *not* space-filling. Based on observations of sheet-like structures in the solar wind (e.g.

<sup>2</sup> The part of the cascade that does not involve the modulation defects involves sharpening in scale, which was linked by Chandran et al. (2015) to collisions between aligned Alfvénic wave packets. They showed analytically that the amplitude of the fluctuations did not change in the collisions between aligned wave packets, which is why equation (10) need not include a scale-dependent factor as the equivalent expression did in the hydrodynamic turbulence model of She & Waymire (1995).

<sup>3</sup> Note that a similar argument for  $\delta z_\lambda$  is somewhat less straightforward because it would require constructing a refined-similarity hypothesis starting from the first equality in equation (2) and letting  $\tau_c \sim \tau_{nl}$ , with  $\tau_{nl}$  given by equation (3) (as was done by Chandran et al. 2015). The resulting relationship between  $\delta z_\lambda$  and  $\epsilon_\lambda$  (whose logarithm is infinitely divisible by the same argument as explained above) then involves the alignment angle, whose distribution is a priori unknown.

Greco et al. 2009; Perri et al. 2012; Osman et al. 2014; Chasapis et al. 2015) and in numerically simulated turbulence, as well as theoretical considerations (e.g. Boldyrev 2006; Zhdankin et al. 2013; Chandran et al. 2015; Howes 2015; Zhdankin, Boldyrev & Uzdensky 2016a), we propose

**Conjecture 2.** *The most intense structures are sheets transverse to the local perpendicular direction.*

Mathematically, this means that if we condition our distribution (11) on  $\hat{\lambda}$  (i.e. restrict ourselves to consider only field increments across both the mean- and the fluctuating-field directions), we must find that the filling fraction of the most intense structures is

$$P(q = 0|\hat{\lambda}) \propto \hat{\lambda}. \quad (19)$$

We will find use for this requirement in Section 3.2, but, since our distribution is formulated most compactly in terms of amplitudes conditional on  $l_{\parallel}$ , equation (15), the most accessible quantity for us is, in fact,

$$P(q = 0|\hat{l}_{\parallel}) = e^{-\mu(\hat{l}_{\parallel})} \quad (20)$$

and so we can determine  $\mu(\hat{l}_{\parallel})$  if we can determine the filling fraction of our sheets as a function of  $\hat{l}_{\parallel}$ . Namely, anticipating

$$P(q = 0|\hat{l}_{\parallel}) \propto \hat{l}_{\parallel}^{\sigma}, \quad (21)$$

we obtain

$$\mu(\hat{l}_{\parallel}) = -\sigma \ln \hat{l}_{\parallel}. \quad (22)$$

### 3.1 Finding $\sigma$ : refined critical balance

Consider what we expect the filling fraction of the singular sheets to be conditionally on  $\hat{l}_{\parallel}$ . By integrating out  $\hat{\lambda}$  (equation 12), we have restricted consideration to field increments  $\delta z$  between point separations that lie in a plane defined by the fluctuation direction and the parallel direction. This restricts us to a plane that is tangent to a ‘flux sheet’ that coherently extends a distance  $l_{\parallel}$  along the mean-magnetic-field direction and a distance  $\xi$  along the fluctuation direction (which, by definition, is perpendicular to both  $l_{\parallel}$  and  $\lambda$ ). Therefore, the filling fraction of the sheet within the plane must be

$$P(q = 0|\hat{l}_{\parallel}) \sim \hat{l}_{\parallel} \hat{\xi}. \quad (23)$$

Note that  $\hat{\xi}$  is, by assumption, a function of both  $q$  (i.e. the amplitude  $\delta z$ ) and  $\hat{l}_{\parallel}$  (see equation 4), but we are about to argue that for  $q = 0$  it only depends on  $\hat{l}_{\parallel}$ .

We now postulate the ‘refined critical balance’, a conjecture inspired by numerical evidence (Mallet et al. 2015):

**Conjecture 3.** *The ratio of linear to nonlinear time-scales (see equation 6)*

$$\chi \doteq \frac{\delta z l_{\parallel}}{\xi v_A} = \left( \frac{L_{\parallel}}{L_{\perp}} \frac{\delta z}{v_A} \right) \beta^q \frac{\hat{l}_{\parallel}}{\hat{\xi}} \quad (24)$$

*is statistically independent of scale.*

This implies that for the most intense fluctuations, which have  $q = 0$ ,

$$\hat{\xi} \sim \hat{l}_{\parallel}, \quad (25)$$

or, to be precise, the ratio  $\hat{l}_{\parallel}/\hat{\xi}$  has a probability distribution that is statistically independent of scale. We therefore posit that equation (23) becomes

$$P(q = 0|\hat{l}_{\parallel}) \propto \hat{l}_{\parallel}^2, \quad (26)$$

i.e.  $\sigma = 2$  in equation (21). Consequently, from equation (22),

$$\mu(\hat{l}_{\parallel}) = -2 \ln \hat{l}_{\parallel}. \quad (27)$$

Note that some circumstantial evidence in support of equation (25) has recently been reported by Zhdankin et al. (2016a), who find that the lengths (our  $l_{\parallel}$ ) and widths (our  $\xi$ ) of Elsasser-vorticity (current) structures in their numerical simulations have a joint distribution peaked at  $l_{\parallel} \propto \xi$ .

### 3.2 Finding $\alpha$

To find  $\alpha$ , we will use equation (19), and so we must first calculate

$$P(q|\hat{\lambda}) = \frac{P(q, \hat{\lambda})}{P(\hat{\lambda})}. \quad (28)$$

Integrating equation (13) over  $\hat{l}_{\parallel}$ , we obtain

$$P(\hat{\lambda}) = \int_0^1 f\left(\frac{\hat{l}_{\parallel}}{\hat{\lambda}^{\alpha}}\right) d\hat{l}_{\parallel} = \hat{\lambda}^{\alpha} \int_0^{1/\hat{\lambda}^{\alpha}} f(y) dy. \quad (29)$$

Using equation (27) and integrating equation (11) over  $\hat{l}_{\parallel}$ , we obtain

$$\begin{aligned} P(q, \hat{\lambda}) &= \int_0^1 \frac{[-2 \ln \hat{l}_{\parallel}]^q}{q!} \hat{l}_{\parallel}^2 f\left(\frac{\hat{l}_{\parallel}}{\hat{\lambda}^{\alpha}}\right) d\hat{l}_{\parallel} \\ &= \hat{\lambda}^{3\alpha} \int_0^{1/\hat{\lambda}^{\alpha}} \frac{[-2 \ln(y \hat{\lambda}^{\alpha})]^q}{q!} y^2 f(y) dy. \end{aligned} \quad (30)$$

With equations (30) and (29), equation (28) gives us

$$P(q|\hat{\lambda}) = \frac{\hat{\lambda}^{2\alpha} \int_0^{1/\hat{\lambda}^{\alpha}} [-2 \ln(y \hat{\lambda}^{\alpha})]^q y^2 f(y) dy}{q! \int_0^{1/\hat{\lambda}^{\alpha}} f(y) dy}. \quad (31)$$

This is a weighted mixture of Poisson distributions with different means. The probability (filling fraction) of the most intense structures conditional on  $\hat{\lambda}$  is, therefore,

$$P(q = 0|\hat{\lambda}) = \hat{\lambda}^{2\alpha} \frac{\int_0^{1/\hat{\lambda}^{\alpha}} y^2 f(y) dy}{\int_0^{1/\hat{\lambda}^{\alpha}} f(y) dy}. \quad (32)$$

Suppose that  $f(y)$  decays fast enough so, at most,

$$f(y) = O\left(\frac{1}{y^{\delta+3}}\right) \text{ for } \delta > 0 \text{ as } y \rightarrow \infty. \quad (33)$$

Then, in the inertial range, i.e. for  $\hat{\lambda} \ll 1$  (in the limit of large Reynolds numbers), equation (31) becomes

$$P(q = 0|\hat{\lambda}) \approx C \hat{\lambda}^{2\alpha}, \quad (34)$$

where

$$C = \frac{\int_0^{\infty} y^2 f(y) dy}{\int_0^{\infty} f(y) dy} = \text{const.} \quad (35)$$

Comparing equations (34) and (19), we conclude that

$$\alpha = \frac{1}{2}. \quad (36)$$

Besides enabling us to fix the parameters of our model (11), this result will have interesting and checkable consequences, which will be examined in Section 6.

We now have a complete expression for our joint probability distribution (11):

$$P(q, \hat{l}_{\parallel}, \hat{\lambda}) = \frac{(-2 \ln \hat{l}_{\parallel})^q}{q!} \hat{l}_{\parallel}^2 f\left(\frac{\hat{l}_{\parallel}}{\hat{\lambda}^{1/2}}\right). \quad (37)$$

It remains to determine the parameter  $\beta$ , which determines the relationship between  $q$  and  $\delta\hat{z}$  (equation 10), and hence calculate all desired scalings.

## 4 SCALINGS

### 4.1 Finding $\beta$ : parallel cascade

To find  $\beta$ , we use the constant-flux hypothesis (2), combined with the critical-balance hypothesis and formalised as follows.

**Conjecture 4.** *The mean flux of energy is constant through parallel scales in the inertial range:*

$$\epsilon = \frac{\langle \delta z^2 | l_{\parallel} \rangle v_A}{l_{\parallel}} = \text{const.} \quad (38)$$

Let us calculate  $\langle \delta z^n | \hat{l}_{\parallel} \rangle$  by multiplying equation (15) by  $\delta z^n = \beta^{nq}$ , summing over  $q$ , and using equation (22):

$$\langle \delta z^n | \hat{l}_{\parallel} \rangle = \sum_{q=0}^{\infty} \beta^{nq} \frac{\mu^q}{q!} e^{-\mu} = e^{-\mu(1-\beta^n)} = \hat{l}_{\parallel}^{\sigma(1-\beta^n)}. \quad (39)$$

Fitting the case of  $n = 2$  to equation (38), we obtain a simple equation for  $\beta$ ,

$$\sigma(1 - \beta^2) = 1, \quad (40)$$

whose positive solution for  $\sigma = 2$  (equation 27) is

$$\beta = \frac{1}{\sqrt{2}}. \quad (41)$$

Thus, all the parameters of our model have now been determined.

### 4.2 Parallel structure functions

In equation (39), we already calculated the scaling exponents of the parallel conditional structure functions: defining  $\zeta_n^{\parallel}$  by

$$\langle \delta z^n | l_{\parallel} \rangle \propto l_{\parallel}^{\zeta_n^{\parallel}}, \quad (42)$$

we find

$$\zeta_n^{\parallel} = \sigma(1 - \beta^n) = 2 \left( 1 - \frac{1}{2^{n/2}} \right). \quad (43)$$

The second-order exponent is

$$\zeta_2^{\parallel} = 1 \quad (44)$$

(by assumption; see Section 4.1), implying the parallel spectral index of  $-2$  (Goldreich & Sridhar 1997).

### 4.3 Perpendicular structure functions

To find the scaling exponents  $\zeta_n^{\perp}$  of the perpendicular structure functions,

$$\langle \delta z^n | \lambda \rangle \propto \lambda^{\zeta_n^{\perp}}, \quad (45)$$

we multiply equation (31) by  $\delta z^n = \beta^{nq}$ , and sum over  $q$ :

$$\begin{aligned} \langle \delta z^n | \hat{\lambda} \rangle &= \frac{\hat{\lambda}^{2\alpha} \int_0^{1/\hat{\lambda}^\alpha} \sum_{q=0}^{\infty} \frac{[-2\beta^n \ln(y\hat{\lambda}^\alpha)]^q}{q!} y^2 f(y) dy}{\int_0^{1/\hat{\lambda}^\alpha} f(y) dy}, \\ &= \hat{\lambda}^{2\alpha(1-\beta^n)} \frac{\int_0^{1/\hat{\lambda}^\alpha} y^{2(1-\beta^n)} f(y) dy}{\int_0^{1/\hat{\lambda}^\alpha} f(y) dy} \\ &\approx C_n \hat{\lambda}^{2\alpha(1-\beta^n)}. \end{aligned} \quad (46)$$

The last equality holds in the inertial range, i.e. in the limit  $\hat{\lambda} \ll 1$ , with

$$C_n = \frac{\int_0^{\infty} y^{2(1-\beta^n)} f(y) dy}{\int_0^{\infty} f(y) dy} = \text{const.} \quad (47)$$

Since  $\beta = 1/\sqrt{2} < 1$ , the integrals converge provided that the condition (33) holds. Finally, using  $\alpha = 1/2$  (equation 36), we have the perpendicular scaling exponents:

$$\zeta_n^{\perp} = 2\alpha(1 - \beta^n) = 1 - \frac{1}{2^{n/2}}. \quad (48)$$

The second-order exponent is

$$\zeta_2^{\perp} = \frac{1}{2}, \quad (49)$$

implying the perpendicular spectral index of  $-3/2$  (cf. Boldyrev 2006).

### 4.4 Fluctuation-direction structure functions

The scalings of the structure-functions conditional on  $\xi$ ,

$$\langle \delta z^n | \xi \rangle \propto \xi^{\zeta_n^{\text{fluc}}}, \quad (50)$$

are harder to determine because  $\xi$  depends on the amplitude  $\delta z$  as well as on  $l_{\parallel}$  (see equation 4). Rather than taking this into account rigorously,<sup>4</sup> we will employ a simple ruse.

Let us assume that the fluctuations that provide the dominant contribution to the  $n$ th-order structure-function conditional on  $l_{\parallel}$  are also those that provide the dominant contribution to the structure-function conditional on  $\xi$ . Let  $\delta z_{\text{eff},n}$  be the amplitude of these fluctuations, namely, by definition,

$$\delta z_{\text{eff},n} = \langle \delta z^n | l_{\parallel} \rangle^{1/n} \propto l_{\parallel}^{\zeta_n^{\parallel}/n}. \quad (51)$$

Motivated by equation (24), we now posit that these fluctuations have scale  $\xi_{\text{eff},n}$  in the fluctuation direction, given by

$$\xi_{\text{eff},n} = \frac{\delta z_{\text{eff},n} l_{\parallel}}{v_A} \propto l_{\parallel}^{1+\zeta_n^{\parallel}/n}. \quad (52)$$

Then, from equation (51),

$$(\delta z_{\text{eff},n})^n \propto \xi_{\text{eff},n}^{\zeta_n^{\text{fluc,eff}}}, \quad (53)$$

where, using equation (43),

$$\zeta_n^{\text{fluc,eff}} = \frac{\zeta_n^{\parallel}}{1 + \zeta_n^{\parallel}/n} = \frac{n(1 - \beta^n)}{n/\sigma + 1 - \beta^n} = \frac{n(1 - 1/2^{n/2})}{n/2 + 1 - 1/2^{n/2}}. \quad (54)$$

For lack of a more quantitative theory, we will consider these to be an acceptable approximation of the exponents  $\zeta_n^{\text{fluc}}$  defined by equation (50). The second-order exponent is

$$\zeta_2^{\text{fluc,eff}} = \frac{2}{3}, \quad (55)$$

implying the fluctuation-direction spectral index of  $-5/3$  (cf. Boldyrev 2006). Note also that as  $n \rightarrow \infty$ ,

$$\zeta_n^{\text{fluc,eff}} \approx \zeta_n^{\parallel} \rightarrow 2 \quad \text{as } n \rightarrow \infty. \quad (56)$$

This is in line with the idea that  $\xi \propto l_{\parallel}$  for the most intense structures, which dominate the structure function as  $n \rightarrow \infty$  (see Section 3.1). Thus, while equation (54) is not much more than a useful mnemonic,

<sup>4</sup> Which can perhaps be done via equation (24), but leads to unilluminating and ultimately unrewarding calculations.



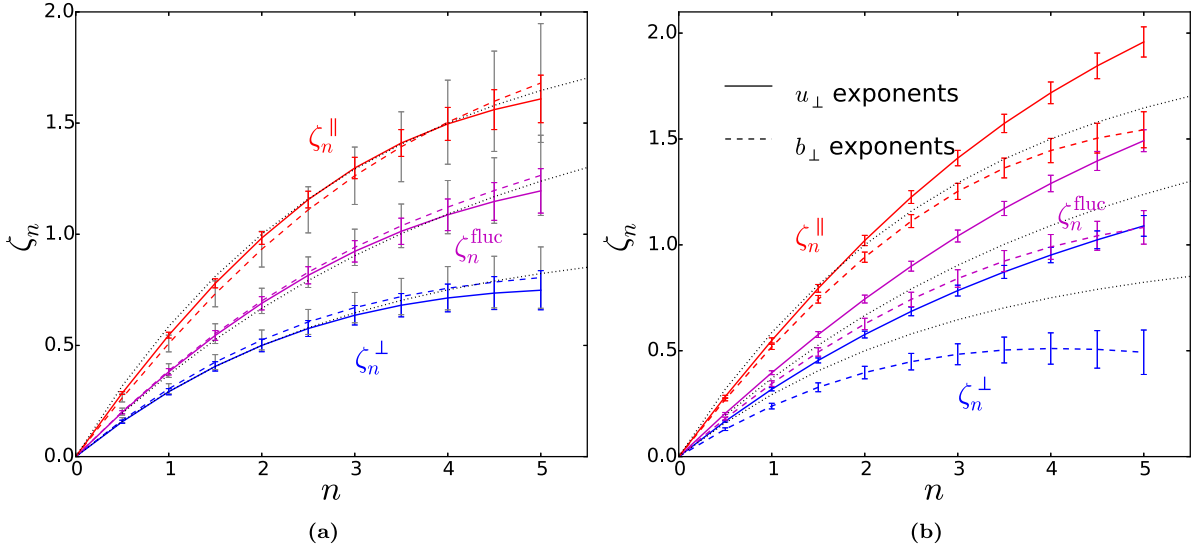


**Figure 1.** (a) Scaling exponents of the  $n$ th-order structure functions of  $z_{\perp}^{+}$  calculated from a  $1024^3$  RMHD numerical simulation of Mallet et al. (2016) are shown as solid lines (see their fig. 1B, showing how the scaling exponents were fitted). They correspond to point separations within  $10^\circ$  of the perpendicular ( $\perp$ , blue), fluctuation ( $\text{fluc}$ , purple) and parallel ( $\parallel$ , red) directions ( $10^\circ$  in the context of the parallel direction refer to angles calculated using lengths in code units; see footnote). The dotted lines are theoretical predictions given by equations (48), (43) and (54). Error bars are standard deviations calculated from data from 10 snapshots separated by more than a turnover time. For further details, see Mallet et al. (2016). To illustrate the level of numerical convergence (or otherwise) of these results, we also show (as dashed lines with grey error bars) the scaling exponents obtained from a smaller,  $512^3$ , but otherwise identical, simulation. (b) Scaling exponents for velocity  $u_{\perp}$  (solid lines) and magnetic field  $b_{\perp}$  (dashed lines) for the same  $1024^3$  simulation. The fluctuation direction in each case is aligned with the field for which the exponents are calculated. See the discussion in Section 5.1.

it behaves in a physically transparent way and, as we are about to see also works quite well, so we consider it worthwhile, even if a more sophisticated theory is undoubtedly conceivable.

## 5 NUMERICAL TESTS

### 5.1 Structure-function scaling exponents

To evaluate how well our model can describe available data, we compare the scaling exponents given by equations (43), (48) and (54) to those measured using conditional structure functions calculated for the  $1024^3$  RMHD numerical simulation described in detail in Mallet et al. (2016). The scaling exponents measured in the simulation are reproduced in Fig. 1a and show very reasonable agreement with our model. We refer the reader to Chandran et al. (2015) for a review and discussion of earlier numerical and observational measurements of the structure-function exponents. Note in particular that results obtained in full-MHD (e.g. Müller, Biskamp & Grappin 2003), rather than RMHD simulations, do not appear to be converged with respect to the asymptotically large size of the mean field, which in RMHD is analytically hard-wired by the underlying ordering. As the size of the mean field was increased, their measured high  $n$  scaling exponents decrease, towards those of our model.

In Fig. 1b, we give the scaling exponents for the velocity and magnetic fields (to contrast them with those for the Elsasser fields in Fig. 1a). These do not coincide with either each other ( $b_{\perp}$  is ‘more intermittent’ than  $u_{\perp}$ ) or with the scalings for the Elsasser fields and are not well described by our equations (43), (48) and (54). This is not a particular problem for our theory, which does not claim to be able to predict these scalings – indeed, to do this, we would have had to construct a model for the *joint* distribution of  $\delta z_{\perp}^{+}$  and  $\delta z_{\perp}^{-}$  within any given fluctuation (i.e. a statistical model of ‘local imbalance’ in RMHD turbulence). Presumably, the fact that the velocity

and magnetic-field perturbations have different scaling properties than the Elsasser fields means that all these fields cannot simply be assumed to be aligned with each other with alignment angles that have similar scale dependence (cf. Perez & Boldyrev 2009). It is indeed a known property of numerical MHD turbulence that alignment angles between different fields can differ (Beresnyak & Lazarian 2006, 2009; Mason, Cattaneo & Boldyrev 2006). They can also differ in the MHD fluctuations measured in space (Wicks et al. 2013a,b). Some theoretical predictions of various alignment angles can be found in Chandran et al. (2015).

### 5.2 Distribution of parallel increments

Let us now attempt a more sensitive test and check whether the distribution of the fluctuation amplitudes conditional on the parallel scale is consistent with our log-Poisson model (15). We do this by directly calculating the distribution of the *parallel* increments of the Elsasser field produced by our numerical simulation. Namely, in view of equation (10), we consider the random variable

$$q = \frac{\ln(\delta z_{l_{\parallel}}^{+}/\overline{\delta z})}{\ln \beta}, \quad (57)$$

where  $\beta = 1/\sqrt{2}$ , as per equation (41), and  $\delta z_{l_{\parallel}}^{+}$  is a field increment across point separation  $l_{\parallel}$  within  $10^\circ$  of the direction parallel to the local mean field.<sup>5</sup> We treat  $\overline{\delta z}$  as a *scale-independent* fitting parameter, determined by a least-squares linear fit between the mean

<sup>5</sup> Angles are calculated formally using lengths in code units. In theory, in RMHD, the box is infinitely elongated and so the parallel units of length are arbitrarily rescalable with respect to the perpendicular ones as long as  $v_A$  is rescaled by the same factor. In the code units, our box is cubic, with  $L_{\perp} = L_{\parallel} = 2\pi$ . The ‘local mean field’ is defined in the same way as in equation (63).

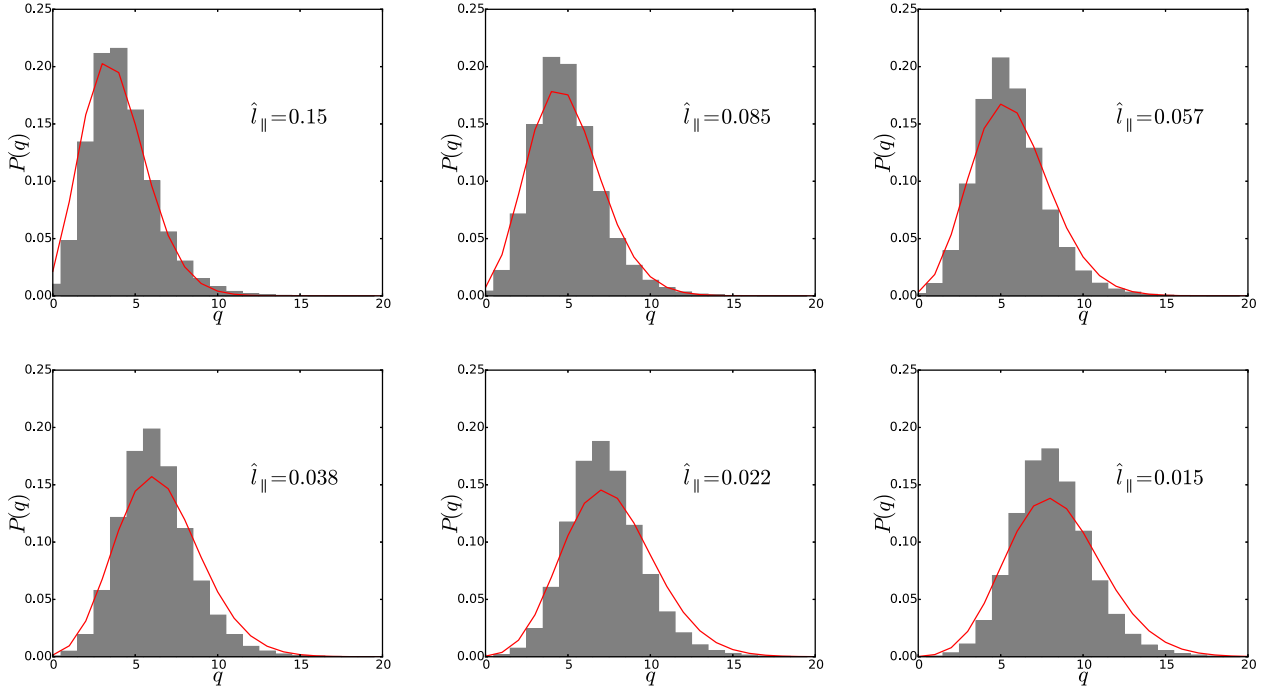


**Figure 2.** Probability distributions of the random variable  $q$  defined in equation (57), calculated from the same simulation as in Fig. 1, are shown as grey bars for six scales:  $\hat{l}_{\parallel} = 0.15, 0.085, 0.057, 0.038, 0.022, 0.015$ ;  $\hat{l}_{\parallel}$  is normalized to the parallel box size ( $L_{\parallel} = 2\pi$  in code units). These scales approximately cover the inertial range (the plots of the structure functions versus scale can be found in Mallet et al. 2016). Red solid lines show the Poisson distribution (15) with mean  $\langle q \rangle = \mu = -2 \ln \hat{l}_{\parallel}$  (equation 27) for those values of  $\hat{l}_{\parallel}$ . Based on equation (58) applied to 17 logarithmically spaced scales (six of which are shown in this figure) in the inertial interval  $\hat{l}_{\parallel} \in [0.015, 0.15]$ , the best-fitting value  $\bar{\delta z} = 9.68$  was found (in code units; in the same units, the rms value of the Elsasser field was  $\langle |z_{\perp}^+|^2 \rangle^{1/2} = 3.32$ ). Note that, while no special measures were taken to ensure that  $q \geq 0$ , there were virtually no increments with  $q < 0$ .

of the distribution of  $\ln \delta z_{\parallel}^+$ , and the mean expected from our model,  $\langle q \rangle = \mu$ , or, using equation (27),

$$\langle \ln \delta z_{\parallel}^+ \rangle = \ln \bar{\delta z} - 2 (\ln \hat{l}_{\parallel}) \ln \beta. \quad (58)$$

Here, we have naively taken  $L_{\parallel} = 2\pi$ , the size of the box in code units (which is the forcing scale in our simulation), and normalized  $\hat{l}_{\parallel} = l_{\parallel}/L_{\parallel}$ . The fit is done for a number of values of  $\hat{l}_{\parallel}$ , covering the extent of the inertial range in the simulation. Thus, we are fitting an entire family of scale-dependent distributions using a single scale-independent parameter, so finding them at least consistent with our log-Poisson model (15) would be a non-trivial and encouraging result.

This is indeed the result that we find: the numerically computed distributions for several values of  $\hat{l}_{\parallel}$  from our inertial interval are shown in Fig. 2, superimposed on the theoretical curves tracing the model distribution (15) with its mean  $\mu$  given by equation (27). The agreement is reasonable, especially with regard to the position of the mean. The high- $q$  tails of the distributions agree slightly less well, which we believe to be due to a systematic underrepresentation of the high- $q$  structures with the two-point field increments,<sup>6</sup> as the contribution to the total field increment due to these structures can be small compared to the contribution

from a Taylor expansion of the fields associated with structures at larger scales but having lower  $q$ . Another source of errors may be an insufficiently precise identification of the direction parallel to the local mean field. Note at any rate that high values of  $q$  do not contribute strongly to the (large- $n$ ) structure functions because they correspond to *lower* amplitudes. This is presumably why the scaling exponents in the numerical simulation (Fig. 1a) are captured so well by our model.

We stress that the log-Poisson fit that we have obtained for  $\delta z_{\parallel}$  is quite good, compared, for example, to the outcome of a similar procedure attempting to fit *perpendicular* increments  $\delta z_{\perp}$  to a log-Poisson model, as carried out, e.g. by Zhdankin et al. (2016b): they point out that, whereas the log-Poisson model for structure-function scaling exponents works well, the distribution of the field increments itself is not well fitted by a log-Poisson curve; we find the same in our own numerical simulation. In our model, however, this is not a problem because the distribution of the logarithms of the perpendicular field increments, equation (31), is a Poisson mixture rather than a pure Poisson distribution. This might be viewed as a piece of circumstantial evidence in support of our argument (in Section 2.2) that the parallel field increments are, via the constant-flux and critical-balance assumptions, more directly related to the infinitely divisible (and, therefore, likely log-Poisson) dissipation field than the perpendicular ones (see footnote 3).

<sup>6</sup> We note that two-point increments of a continuous Elsasser field are not strictly the same thing as amplitudes of notional individual ‘structures’ or ‘fluctuations’ of which our model ‘RMHD ensemble’ consists (see Section 2). We do, however, use two-point increments as the most convenient and simple way to probe fluctuations at a particular scale and implicitly

assume that these should have the same statistics. Clearly, such a correspondence can only be approximate.

## 6 DISTRIBUTION OF ANISOTROPY

The joint distribution of  $l_{\parallel}$  and  $\lambda$  is given by equation (13). It characterizes the scale-dependent anisotropy of the turbulent structures in the RMHD ensemble. Using equation (29), we find that, in the inertial range (where  $\hat{\lambda} \ll 1$ ),

$$P(\hat{l}_{\parallel}|\hat{\lambda}) = \frac{P(\hat{l}_{\parallel}, \hat{\lambda})}{P(\hat{\lambda})} \approx \frac{f(\hat{l}_{\parallel}/\hat{\lambda}^{\alpha})}{\hat{\lambda}^{\alpha} I}, \quad (59)$$

where  $I = \int_0^{\infty} f(y)dy$ , which we assume converges. Changing variables from  $\hat{l}_{\parallel}$  to  $y = \hat{l}_{\parallel}/\hat{\lambda}^{\alpha}$ , we find

$$P(y|\hat{\lambda}) = \frac{f(y)}{I}. \quad (60)$$

Thus, our (thus far unknown) function  $f$  is just the probability density function of  $y$ , which is independent of  $\hat{\lambda}$  (i.e.  $y$  has scale-invariant statistics). This means that, for field increments deep enough into the inertial range,

$$\hat{l}_{\parallel} \sim \hat{\lambda}^{\alpha}. \quad (61)$$

This is, of course, also why our equations (48) and (43) had the property

$$\zeta_n^{\parallel} = 2\zeta_n^{\perp}, \quad (62)$$

which we showed in Fig. 1 to be approximately true in numerically simulated RMHD turbulence.

Let us now measure the distribution of the anisotropy directly. We follow Mallet et al. (2015), who defined the parallel coherence length  $l_{\parallel}$  for a given perpendicular increment  $\lambda$  between spatial positions  $\mathbf{r}_0$  and  $\mathbf{r}_0 + \mathbf{r}_{\perp}$  (where  $|\mathbf{r}_{\perp}| = \lambda$ ) as the distance along the *perturbed* field line at which the Elsasser-field increment is the same as the perpendicular increment (Cho & Vishniac 2000; Maron & Goldreich 2001; Matthaeus et al. 2012):

$$\left| \mathbf{z}_{\perp}^{\pm} \left( \mathbf{r}_0 + \frac{\mathbf{r}_{\perp} + l_{\parallel} \hat{\mathbf{b}}_{\text{loc}}}{2} \right) - \mathbf{z}_{\perp}^{\pm} \left( \mathbf{r}_0 + \frac{\mathbf{r}_{\perp} - l_{\parallel} \hat{\mathbf{b}}_{\text{loc}}}{2} \right) \right| = |\mathbf{z}_{\perp}^{\pm}(\mathbf{r}_0 + \mathbf{r}_{\perp}) - \mathbf{z}_{\perp}^{\pm}(\mathbf{r}_0)|, \quad (63)$$

where  $\hat{\mathbf{b}}_{\text{loc}} = \mathbf{B}_{\text{loc}}/|\mathbf{B}_{\text{loc}}|$  is the unit vector along the ‘local mean field’  $\mathbf{B}_{\text{loc}} \doteq \mathbf{B}_0 + [\mathbf{b}_{\perp}(\mathbf{r}_0) + \mathbf{b}_{\perp}(\mathbf{r}_0 + \mathbf{r}_{\perp})]/2$ . Using this definition, we can measure the distribution of  $l_{\parallel}$  as a random variable conditional on  $\lambda$ . The resulting rescaled distribution of  $y = l_{\parallel}/\lambda^{1/2}$  is shown in Fig. 3. Both the core of the distribution and the ‘typical’ values of  $l_{\parallel}$  (defined in terms of a logarithmic average) appear to support the corollaries of our model that  $y$  is scale invariant and  $\alpha = 1/2$ . There is a minority population of fluctuations with relatively larger  $l_{\parallel}$  and  $\lambda$  that do not appear to obey this rescaling, which suggests an imperfection of our model (unless it is a box-size convergence issue). However, this minority is small, which explains why it does not affect inertial-range scalings reported in Section 5.1.

In view of equation (60), the probability density function plotted in Fig. 3 gives us an idea as to the shape of the function  $f(y)$ . Remarkably, at larger  $y$ , it scales very precisely as<sup>7</sup>

$$f(y) \sim \frac{1}{y^3}. \quad (64)$$

<sup>7</sup> Zhankin et al. (2016a) appear to have observed a not entirely dissimilar scaling for the lengths and widths of Elsasser-vorticity (current) sheets in their numerical simulations of MHD turbulence. These should correspond to our  $l_{\parallel}$  and  $\xi$  variables (which indeed have the same distribution for the most intense structures; see Section 3.1) – although Zhankin et al. (2016a) have a completely different scheme for measuring them.

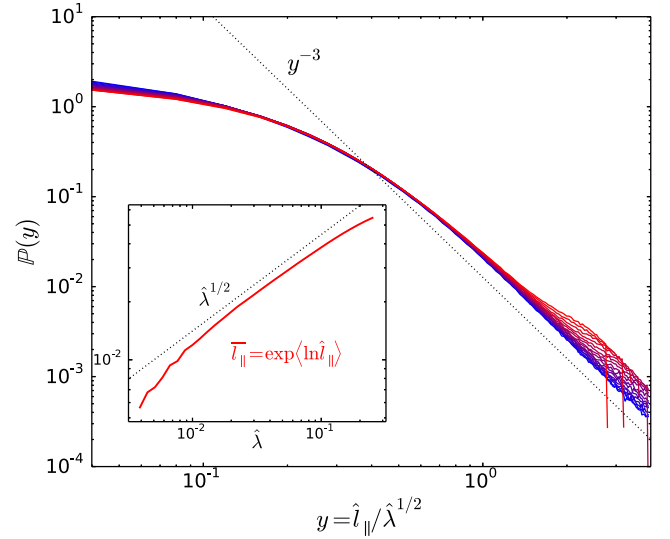


**Figure 3.** The distribution of  $y = \hat{l}_{\parallel}/\hat{\lambda}^{1/2}$  for  $\mathbf{z}_{\perp}^+$ , calculated in the same simulation as in Fig. 1. Here,  $\hat{l}_{\parallel}$  and  $\hat{\lambda}$  are normalized to box size in the parallel ( $L_{\parallel} = 2\pi$  in code units) and perpendicular ( $L_{\perp} = 2\pi$  in code units) directions, respectively (which were also the scales at which the turbulence was forced; see Mallet et al. 2016). The range of perpendicular scales is from  $\hat{\lambda} = 0.015$  (blue/dark lines) to  $\hat{\lambda} = 0.15$  (red/light lines). The dotted line shows the critical scaling  $f \propto y^{-3}$  (see condition 33). Inset: the ‘typical’ parallel scale obtained via logarithmic average  $\bar{l}_{\parallel} = \exp \langle \ln \hat{l}_{\parallel} \rangle$ ; the  $\bar{l}_{\parallel} \propto \lambda^{1/2}$  scaling is shown by the dotted line.

This is the ‘fattest’ tail allowed by the condition (33), which we needed to be satisfied in order for our derivation of the  $\hat{\lambda}$  scaling of  $P(q=0|\hat{\lambda})$  in Section 3.2 to be valid. If the tail were any fatter, the integral in the numerator of equation (32) would be dominated by the upper limit and so the scaling of  $P(q=0|\hat{\lambda})$  with  $\hat{\lambda}$  would depend not just on  $\alpha$ , but also on the asymptotic form of  $f(y)$ . In view of the result (64), our derivation survives, subject at most to a logarithmic correction (which, at this level of modelling, we view as irrelevant). It is an interesting question whether there is some compelling mechanism whereby the distribution of the anisotropy is allowed to be as broad as this but no broader.

## 7 DISCUSSION

The model of strong Alfvénic turbulence presented in this paper leads to anisotropic scalings of the conditional structure functions in the local physical directions parallel to the local magnetic field, along the direction of the local fluctuation, and perpendicular to both of those, consistent with numerical evidence previously reported by Mallet et al. (2016). To achieve this, we have proposed four physically motivated conjectures: that the fluctuation amplitudes have an ‘anisotropic log-Poisson’ distribution (cf. Chandran et al. 2015; Zhankin et al. 2016b), that the structures are sheet-like (cf. Zhankin et al. 2013, 2016a; Chandran et al. 2015; Howes 2015), that the critical-balance parameter (including dynamic alignment) is independent of scale (Mallet et al. 2015), and finally that there is a constant flux of energy through parallel scales in the inertial range (cf. Beresnyak 2015). This allows us to fix all the parameters of the model, resulting in simple predictions for the scalings of  $n$ th-order conditional structure functions in the perpendicular and parallel directions. In the fluctuation direction, we find the scalings approximately using an additional assumption. In all three directions, the scalings agree well with those previously reported



in Mallet et al. (2016) on the basis of numerical simulations (see Section 5). Moreover, we find reasonable agreement between the distribution of parallel field increments in the numerically simulated turbulence and our log-Poisson model.

It is interesting to note that the predicted structure-function scalings in the perpendicular direction are nearly identical to those proposed by Chandran et al. (2015); the only difference being that in their model, the parameter  $\beta \approx 0.691$ , whereas in our model in this paper,  $\beta = 1/\sqrt{2} \approx 0.707$ . This is perhaps not too surprising: both models rely on a log-Poisson model for the fluctuation amplitude, refined critical balance, dynamic alignment and constant flux of energy through scale. The differences are in certain details: first, in order to fix the scalings, Chandran et al. (2015) constructed a detailed dynamical model for the collision of high-amplitude and low-amplitude fluctuations, whereas here we fixed the free parameters of our model via assumptions about the spatial dimensionality of the most intense fluctuations; secondly, for Chandran et al. (2015), the central quantity was the Elsasser-field increment at a given perpendicular point separation  $\lambda$ , whereas here most of the physical assumptions were about field increments at given parallel point separations  $l_{\parallel}$ <sup>8</sup> – these assumptions were then used to model the ‘RMHD turbulent ensemble’ of structures of random amplitudes and sizes in all three spatial directions.

Having an explicit statistical model for such an ensemble then naturally allowed us to predict exponents not just in the perpendicular but also in the parallel and fluctuation directions. We have also been able to predict the distribution of the anisotropy between the parallel and perpendicular scales of the fluctuations: we have argued that, typically in the ensemble,  $l_{\parallel} \sim \lambda^{1/2}$ , independently of the fluctuation amplitude. This was indeed approximately the case in the numerical simulations reported by Mallet et al. (2015, see Section 6).

The scalings that we have derived for the second-order structure functions (equations 49, 44 and 55) and for the relationship between the perpendicular and parallel coherence scales (equations 61 and 36) are the same as proposed by Boldyrev (2006) and, like his, are broadly based on the idea of alignment between fluctuating fields. Note, however, that we have been able to obtain these scalings without the need for the conjecture that the alignment angle is equal to the ‘uncertainty’ in the direction of the fluctuating field ( $\theta \sim \delta z_{\perp}/v_A$ ) – a conjecture that, if taken literally, contradicts the scale invariance property of RMHD equations (Beresnyak 2014). Here, this conjecture has been effectively replaced by Conjectures 1–3 (see Sections 2 and 3), leading to equation (36). Another important nuance is that we are effectively assuming alignment between the Elsasser fields, rather than between the velocity and magnetic fields (cf. Beresnyak & Lazarian 2006, 2009; Mason et al. 2006; Chandran et al. 2015) – whereas the two types of alignment are compatible and have been argued to occur simultaneously (Perez & Boldyrev 2009), they are not mutually necessary and fluctuations with one but not another have been found in the solar wind (Wicks et al. 2013a,b). Our theory cannot and indeed does not predict velocity and magnetic-field scalings, which turn out to be different both from each other and from the Elsasser fields (see Section 5.1). A more refined theory aspiring to explain this behaviour will have to

address the statistical dependence of the two Elsasser fields on each other (i.e. the statistics of ‘local imbalance’ in MHD turbulence).

It is a valid question whether scaling exponents computed from numerical simulations (e.g. the structure-function exponents in Section 5.1) are believable if they are obtained without a systematic study of convergence in the limit of large Reynolds number (which would be the ‘gold standard’ in hydrodynamics; see e.g. Gotoh, Fukayama & Nakano 2002). Indeed, in MHD turbulence such an approach was argued to be a sine qua non by Beresnyak (Beresnyak 2014) and the question what to make of such studies at currently affordable – possibly insufficient – resolutions is a controversial one (Beresnyak 2014; Perez et al. 2014). We are not in position to carry out a numerical study that would exceed in size those already in existence and indeed we do not claim that aligned, 3D-anisotropic RMHD turbulent state that is seen in the numerical simulations at currently available resolutions will necessarily survive to arbitrarily small scales in the limit of  $Re \rightarrow \infty$ . However, it appears that it does persist down to scale separations about a decade below the driving scale, which is the range captured in current simulations and, indeed, is not dramatically less broad than the universal part of the inertial range appears to be in the solar-wind turbulence. We therefore consider having a good model of Alfvénic fluctuations at these scales worthwhile and leave to future work the fascinating but still somewhat murky (and as yet difficult to address numerically) problem of what happens at even smaller scales.

It is fair to observe that in the solar wind, unlike in our model or in numerical simulations, definitive proof of a *scale-dependent* anisotropy in the inertial range between the perpendicular and fluctuation directions (i.e. scale-dependent alignment) has been elusive (Podesta et al. 2009; Chen et al. 2012; Wicks et al. 2013a), in contrast to the anisotropy with respect to the local mean field, which is quite well established (Horbury et al. 2008; Podesta 2009; Wicks et al. 2010; Chen et al. 2011). This could be due to the solar-wind expansion affecting the anisotropy (Verdini & Grappin 2015), reflection of Alfvénic fluctuations close to the Sun (Heinemann & Olbert 1980; Perez & Chandran 2013), or the highly imbalanced nature of the solar-wind turbulence (e.g. Wicks et al. 2011, 2013b). In any event, making quantitative contact between theory and data requires understanding of these effects. We lay no claim to such a complete understanding. Nevertheless, it appears that, by incorporating all three of intermittency, dynamic alignment and critical balance in the same theoretical scheme, our model does at least help to make sense of the 3D-anisotropic statistics found in numerical simulations of homogeneous, balanced Alfvénic turbulence.

## ACKNOWLEDGEMENTS

We are indebted to B. D. G. Chandran for many important discussions, which substantially influenced this work. We also thank A. Beresnyak for useful comments, which helped improve our exposition. The work of AM was supported by National Aeronautics and Space Administration (NASA) grant NNX15AI80G and National Science Foundation (NSF) grants PHY-1500041, AGS-1258998, and AGS-1624501. The work of AAS was supported in part by grants from UK Science and Technologies Facilities Council (STFC) and Engineering & Physical Sciences Research Council (EPSRC). Simulations reported here used Extreme Science and Engineering Discovery Environment (XSEDE), which is supported by the US NSF Grant ACI-1053575. Both authors thank the Wolfgang Pauli Institute, Vienna, where this work was conceived, for its hospitality. We also thank the anonymous referee for their helpful suggestions.

<sup>8</sup> Both the numerical evidence (the log-Poisson fits in Section 5.2) and physical arguments based on the constant-flux and critical-balance assumptions (Section 2.2) suggest that perhaps ‘starting’ with parallel field increments in constructing theories of Alfvénic turbulence is a strategy that has some meaning.

## REFERENCES

- Beresnyak A., 2014, *ApJ*, 784, L20  
 Beresnyak A., 2015, *ApJ*, 801, L9  
 Beresnyak A., Lazarian A., 2006, *ApJ*, 640, L175  
 Beresnyak A., Lazarian A., 2009, *ApJ*, 702, 1190  
 Bigot B., Galtier S., Politano H., 2008, *Phys. Rev. E*, 78, 066301  
 Boldyrev S., 2006, *Phys. Rev. Lett.*, 96, 115002  
 Bruno R., Carbone V., 2013, *Living Rev. Sol. Phys.*, 10, 2  
 Chandran B. D. G., Schekochihin A. A., Mallet A., 2015, *ApJ*, 807, 39  
 Chasapis A. et al., 2015, *ApJ*, 804, L1  
 Chen C. H. K., Mallet A., Yousef T. A., Schekochihin A. A., Horbury T. S., 2011, *MNRAS*, 415, 3219  
 Chen C. H. K., Mallet A., Schekochihin A. A., Horbury T. S., Wicks R. T., Bale S. D., 2012, *ApJ*, 758, 120  
 Cho J., Vishniac E. T., 2000, *ApJ*, 539, 273  
 Dubrulle B., 1994, *Phys. Rev. Lett.*, 73, 959  
 Frisch U., 1995, *Turbulence: The Legacy of A. N. Kolmogorov*. Cambridge Univ. Press, Cambridge  
 Goldreich P., Sridhar S., 1995, *ApJ*, 438, 763  
 Goldreich P., Sridhar S., 1997, *ApJ*, 485, 680  
 Gotoh T., Fukayama D., Nakano T., 2002, *Phys. Fluids*, 14, 1065  
 Greco A., Matthaeus W. H., Servidio S., Chuychai P., Dmitruk P., 2009, *ApJ*, 691, L111  
 Heinemann M., Olbert S., 1980, *J. Geophys. Res.*, 85, 1311  
 Horbury T. S., Forman M., Oughton S., 2008, *Phys. Rev. Lett.*, 101, 175005  
 Howes G. G., 2015, *Phil. Trans. R. Soc. A*, 373, 20140145  
 Kolmogorov A., 1941, *Dokl. Akad. Nauk SSSR*, 30, 301  
 Kolmogorov A. N., 1962, *J. Fluid Mech.*, 13, 82  
 Mallet A., Schekochihin A. A., Chandran B. D. G., 2015, *MNRAS*, 449, L77  
 Mallet A., Schekochihin A. A., Chandran B. D. G., Chen C. H. K., Horbury T. S., Wicks R. T., Greenan C. C., 2016, *MNRAS*, 459, 2130  
 Maron J., Goldreich P., 2001, *ApJ*, 554, 1175  
 Mason J., Cattaneo F., Boldyrev S., 2006, *Phys. Rev. Lett.*, 97, 255002  
 Matthaeus W. H., Ghosh S., Oughton S., Roberts D. A., 1996, *J. Geophys. Res.*, 101, 7619  
 Matthaeus W. H., Oughton S., Ghosh S., Hossain M., 1998, *Phys. Rev. Lett.*, 81, 2056  
 Matthaeus W. H., Servidio S., Dmitruk P., Carbone V., Oughton S., Wan M., Osman K. T., 2012, *ApJ*, 750, 103  
 Müller W.-C., Biskamp D., Grappin R., 2003, *Phys. Rev. E*, 67, 066302  
 Osman K. T., Matthaeus W. H., Gosling J. T., Greco A., Servidio S., Hnat B., Chapman S. C., Phan T. D., 2014, *Phys. Rev. Lett.*, 112, 215002  
 Oughton S., Priest E. R., Matthaeus W. H., 1994, *J. Fluid Mech.*, 280, 95  
 Oughton S., Dmitruk P., Matthaeus W. H., 2004, *Phys. Plasmas*, 11, 2214  
 Perez J. C., Boldyrev S., 2009, *Phys. Rev. Lett.*, 102, 025003  
 Perez J. C., Chandran B. D. G., 2013, *ApJ*, 776, 124  
 Perez J. C., Mason J., Boldyrev S., Cattaneo F., 2014, *ApJ*, 793, L13  
 Perri S., Goldstein M. L., Dorelli J. C., Sahraoui F., 2012, *Phys. Rev. Lett.*, 109, 191101  
 Podesta J. J., 2009, *ApJ*, 698, 986  
 Podesta J. J., Chandran B. D. G., Bhattacharjee A., Roberts D. A., Goldstein M. L., 2009, *J. Geophys. Res.*, 114, 1107  
 Sato K., 2013, *Lévy Processes and Infinitely Divisible Distributions*. Cambridge Univ. Press, Cambridge  
 Schekochihin A. A., Cowley S. C., Dorland W., Hammett G. W., Howes G. G., Quataert E., Tatsuno T., 2009, *ApJS*, 182, 310  
 Shebalin J. V., Matthaeus W. H., Montgomery D., 1983, *J. Plasma Phys.*, 29, 525  
 She Z.-S., Leveque E., 1994, *Phys. Rev. Lett.*, 72, 336  
 She Z.-S., Waymire E. C., 1995, *Phys. Rev. Lett.*, 74, 262  
 Verdini A., Grappin R., 2015, *ApJ*, 808, L34  
 Wicks R. T., Horbury T. S., Chen C. H. K., Schekochihin A. A., 2010, *MNRAS*, 407, L31  
 Wicks R. T., Horbury T. S., Chen C. H. K., Schekochihin A. A., 2011, *Phys. Rev. Lett.*, 106, 045001  
 Wicks R. T., Mallet A., Horbury T. S., Chen C. H. K., Schekochihin A. A., Mitchell J. J., 2013a, *Phys. Rev. Lett.*, 110, 025003  
 Wicks R. T., Roberts D. A., Mallet A., Schekochihin A. A., Horbury T. S., Chen C. H. K., 2013b, *ApJ*, 778, 177  
 Zhdankin V., Uzdensky D. A., Perez J. C., Boldyrev S., 2013, *ApJ*, 771, 124  
 Zhdankin V., Boldyrev S., Uzdensky D. A., 2016a, *Phys. Plasmas*, 23, 055705  
 Zhdankin V., Boldyrev S., Chen C. H. K., 2016b, *MNRAS*, 457, L69

This paper has been typeset from a  $\text{\LaTeX}$  file prepared by the author.